A REDUCED MODEL FOR NEPHRON FLOW DYNAMICS MEDIATED BY TUBULOGLOMERULAR FEEDBACK

E. BRUCE PITMAN*, ROMAN M. ZARITSKI†, LEON C. MOORE‡, AND H. E. LAYTON§

Abstract. Previously we developed a "minimal" mathematical model of the tubuloglomerular feedback (TGF) system in a short-looped nephron of the mammalian kidney. In that model, a hyperbolic partial differential equation (PDE) represented the advection and transepithelial transport of chloride in the thick ascending limb (TAL). The feedback response was represented by an empirical relationship that determined the glomerular filtration rate as a function of time-delayed TAL luminal chloride concentration alongside the macula densa. This PDE model system with feedback and a time delay presents analytical and computational challenges. In this report, we derive a reduced model that is based on the minimal model. The reduced model, which is formulated as an integral equation in time, is easier to study than the PDE model. As in the case of the minimal model, analysis of the reduced model suggests that sustained oscillations in nephron fluid flow arise from a Hopf bifurcation, with delay time and system gain as bifurcation parameters. Both analysis and numerical calculations indicate that the principal bifurcation locus predicted by the reduced model coincides with the analogous locus obtained from the minimal model. Near the principal bifurcation locus, numerical solutions of the two models nearly coincide. For bifurcation parameters that differ sufficiently from the principal bifurcation locus, the numerical solutions to the two models differ somewhat. The reduced TGF model has the potential to facilitate simulation and analysis of interactions among TGF systems in multiple nephrons.

Key words. Mathematical model, functional differential equations, Hopf bifurcation, renal autoregulation, kidney

AMS(MOS) subject classifications. Primary 34K18, 34K28, 92C35; secondary 35L99.

1. Introduction.

Tubuloglomerular feedback (TGF) is an important controller of kidney function. A distinct TGF system operates in each of the nephrons, which are the primary functional units of the kidney. TGF regulates the flow of fluid leaving the proximal parts of a nephron (the proximal tubule and Henle's loop) by monitoring the NaCl concentration of the tubular fluid as it passes the macula densa (MD), a plaque of specialized cells in the wall of the thick ascending limb (TAL) of Henle's loop (see Fig. 1, below). When the MD is stimulated by an increase in the NaCl concentration of the tubular fluid (an increase that normally occurs when TAL fluid flow increases) a signal is directed to the afferent arteriole (AA) that supplies blood to that same nephron. In response, the AA

*Department of Mathematics, State University of New York, Buffalo, NY 14214-3093.

† Department of Mathematics, State University of New York, Buffalo, NY 14214-3093. Present address: Department of Computer Science, Montclair State University, Upper Montclair, NJ 07043.

‡Department of Physiology and Biophysics, State University of New York, Stony Brook, New York 11794-8661.

§Department of Mathematics, Duke University, Durham, North Carolina 27708-0320.

constricts, which reduces the blood flow to, and the hydrostatic pressure within, the glomerular capillaries, resulting in a reduced rate of filtration into the nephron. By this means, TGF balances the load of fluid presented to the nephron with the capacity of tubular epithelial cells to absorb and process the filtered fluid. TGF also participates in the stabilization of renal blood flow and glomerular filtration rate in response to fluctuations in systemic arterial blood pressure, a phenomenon called renal autoregulation [21].

Fluid flow in the nephrons of normotensive rats either approximates a time-independent steady state or exhibits sustained limit-cycle oscillations (LCO) with frequency of about 25-50 mHz [9, 11]. Fluid flow in the nephrons of hypertensive rats often exhibits irregular oscillations that are suggestive of deterministic chaos [22]. Experiments have established that the flow oscillations, whether LCO or irregular oscillations, involve the TGF system [11].

Several mathematical models have been formulated to elucidate the origins of these flow oscillations [1, 8, 10, 13, 18]. In previous work, we formulated a "minimal" dynamic model of fluid flow and solute advection in a nephron [13]. In that model, a hyperbolic partial differential equation (PDE) represents the advection and transepithelial transport of chloride in the TAL. Feedback is represented by an empirical relationship that determines glomerular filtration, and hence TAL flow speed, as a function of the intratubular chloride concentration sensed by the MD at an earlier time. This results in a time-delay PDE. Analysis and numerical computations show that model behavior depends critically on at least two parameters, the delay τ at the MD and the feedback loop gain γ; indeed, the analysis suggests that a Hopf bifurcation occurs along a locus in the τ-γ parameter space [13]. The bifurcation locus marks the loss of stability of time-independent steady-state model solutions and the appearance of stable LCO. The range of physiological parameters measured in the kidneys of normotensive rats is approximately bisected by the bifurcation locus, which may help explain why some nephrons exhibit LCO while others do not. The minimal model is summarized below in Section 2.

The minimal TGF model has been robust in its agreement with experimental data [13, 14, 15, 16, 17]. However, its use of a PDE to describe transport in the TAL limits the possibilities for analysis and presents a significant computational burden in simulation studies involving the interactions of TGF systems in multiple nephrons, a case of considerable physiological importance. Studies in rats show that 50–60% of the superficial nephrons occur in pairs (and some triples), where the afferent arterioles feeding these nephrons branch from a common location, either on a cortical radial artery (CRA) or on a short connecting artery that branches from a CRA [3]. Such nephron pairs (or triplets) are said to have a close vascular connection.

Renal micropuncture experiments have shown that nephron pairs with

close vascular connection, or which branch from discrete sites on the same CRA, usually exhibit synchronous flow oscillations, whereas flow oscillations tend to be uncoordinated in nephron pairs perfused by different CRAs [7]. Yip et al. confirmed that a close vascular coupling of nephron pairs on the CRA is strongly correlated with synchronous oscillations [23]. They also found evidence suggesting that the magnitude of nephron-nephron interaction is greater in hypertensive rats, relative to normotensive animals. Chen et al. verified these findings and found that the strength of the nephron-nephron interaction varies inversely with the length of the vascular structures interposed between the nephrons [5]. Together, these experimental studies provide strong evidence for interaction, or coupling, of nephrons via vascular pathways. The mechanism of vascular coupling most likely involves electrotonic conduction of signals through the gap junctions that connect the smooth muscle and endothelial cells in the AA and CRA [5].

In Ref. [19], we formulated a model for two coupled nephrons as a generalization of our minimal single-nephron model. The two-nephron model contains two hyperbolic PDEs that are coupled via the tubular flows that are determined by the feedback responses. Our investigation shows that an analytical bifurcation analysis is possible for special cases. The results suggest that, by displacing the bifurcation locus, close vascular coupling facilitates the emergence of oscillations, relative to uncoupled nephrons [19]. Numerical simulations further suggest that dynamic behaviors more complex than LCO can be elicited in this model of two coupled nephrons [24]. However, analysis of our TGF models involves the study of bifurcations of a hyperbolic PDE with a time delay—a difficult, non-standard problem in applied mathematics.

In Section 3, we derive from our minimal model a new, "reduced" model of TGF. The reduced model is an integral equation that arises from a linearization of the characteristic form of the original PDE model. Analysis of this reduced model yields the same principal bifurcation locus as the PDE model, and numerical calculations show that the dynamic behaviors of the two models are similar. The reduced model eliminates some of the computational difficulties of the minimal model and thus may be well-suited for studies of inter-nephron interaction.

In Section 4, we derive a functional[1] ordinary differential equation (ODE) that is equivalent to our minimal model, provided that the TAL is assumed to be impermeable to NaCl. This formulation of the minimal model, which has a state-dependent time delay, is helpful for explaining the difficulties inherent in solving the minimal model, relative to the reduced model.

[1] In this context, "functional" means that the differential equation contains a delay in the time variable [6]; such a differential equation is also called a delay differential equation or a differential-difference equation [2].

2. The Minimal Model. In this section, we summarize the minimal model as originally developed in Ref. [13].

2.1. Model formulation. The model represents TGF in a short-looped nephron like that found in the rat. Such nephrons have a loop of Henle that reaches nearly to the boundary of the inner and outer medulla (see Fig. 1). The model is formulated as a system of two coupled equations:

$$\frac{\partial}{\partial t}C(x,t) = -F(C(1,t-\tau))\frac{\partial}{\partial x}C(x,t) - \frac{V_{max}C(x,t)}{K_M + C(x,t)} - P\left(C(x,t) - C_e(x)\right) \tag{2.1}$$

and

$$F(C(1,t-\tau)) = 1 + K_1 \tanh\left(K_2\left(C_{op} - C(1,t-\tau)\right)\right). \tag{2.2}$$

Both equations are expressed in nondimensional form (see *Normalization of equations*, below). The space variable x is oriented so that it extends from the entrance of the TAL ($x = 0$), through the outer medulla, and into the cortex to the MD ($x = 1$).

Equation 2.1, which is based on mass conservation of chloride in a rigid tube, is a PDE for the chloride concentration $C(x,t)$, at position x and time t, in the intratubular fluid of the TAL. At $x = 0$, we assume that $C(0,t) = 1$, meaning that fluid entering the TAL has constant chloride concentration. The rate of change of that concentration for $x \in (0,1]$ depends on processes represented by the three right-hand terms in Eq. 2.1. The first term is axial chloride advection at intratubular flow speed F. The second is transepithelial efflux of chloride driven by active metabolic pumps situated in the tubular walls; that efflux is approximated by Michaelis-Menten kinetics, with maximum transport rate V_{max} and Michaelis constant K_M. The third term is transepithelial chloride backleak, which depends on a specified fixed extratubular chloride concentration profile $C_e(x)$ and on chloride permeability P.

Equation 2.2, which represents the feedback response, gives the TAL intratubular fluid speed as a function of $C(1,\cdot)$, the intratubular TAL chloride concentration alongside the MD (the dot in $C(1,\cdot)$ indicates an arbitrary time). This equation, which was obtained empirically by physiologists, is well-established by steady-state experiments [20]. The constant C_{op} is the steady-state chloride concentration obtained at the MD when $F \equiv 1$. The positive constants K_1 and K_2 describe, respectively, the range of the feedback response and its sensitivity to deviations from the steady state.

Dynamic experiments [4] show that a change in MD concentration does not significantly affect AA muscle tension until after a positive delay time τ. Thus the flow in Eq. 2.1 depends on the MD concentration at the

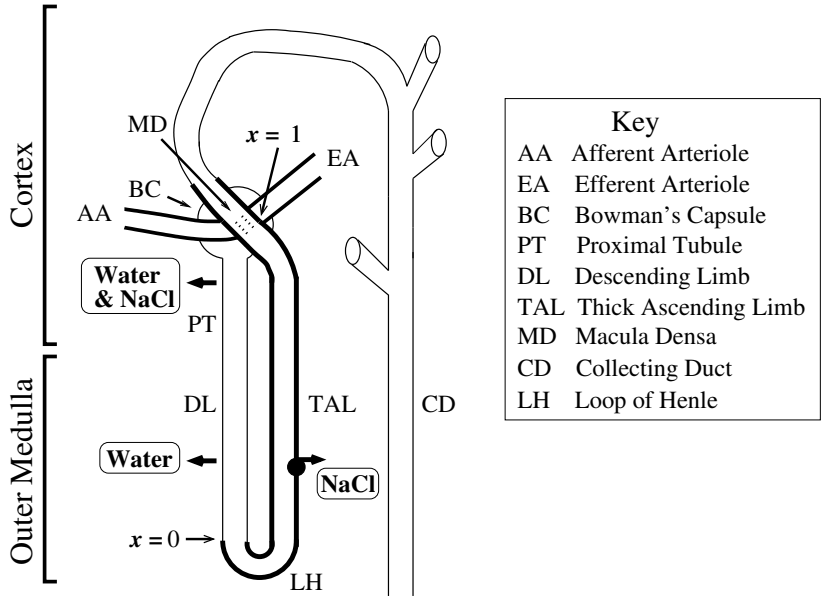

FIG. 1. *Schematic drawing of a short-looped nephron. Relationship to cortex and outer medulla is indicated at left. Important structures are labeled according to Key at right. The glomerulus is contained within Bowman's capsule (BC). The macula densa (MD), contrary to the appearance in this drawing, is on the back side of the thick ascending limb (TAL) and adjacent to the region where the glomerulus, afferent arteriole (AA), and efferent arteriole (EA) come together. Water and NaCl are absorbed from the proximal tubule (PT) and returned to the blood by means of the peritubular capillaries; water is absorbed from the water-permeable descending limb (DL), and NaCl is actively transported from the essentially water-impermeable thick ascending limb (TAL).*

previous time $t - \tau$, i.e., on $C(1, t - \tau)$. At time $t = 0$, the initial TAL concentration profile ($C(x, 0)$ for $x \in (0, 1]$) and a concentration history at the MD ($C(1, t)$ for $t \in [-\tau, 0)$) must be specified.

In this study, which aims at analytical simplification, we will assume that solute backleak, which is perhaps the most important second-order transepithelial transport effect, is zero. Thus, we set $P = 0$ and $C_e(x)$ need not be specified. For subsequent convenience, we write the remaining transepithelial transport term (the one described by Michaelis Menten kinetics) as a function J defined by

$$J(C) = \frac{V_{max} C}{K_M + C}. \tag{2.3}$$

A steady-state solution to Eqs. 2.1 and 2.2 may be obtained by setting $F = 1$ for $t \in [0, 1 + \tau)$. The TAL concentration profile will attain a steady state at $t = 1$, since the TAL transit time is 1 at flow speed 1; moreover, $C(1, t) = C_{op}$ in the interval $t \in [1, 1 + \tau)$. If the feedback loop is closed

at $t = 1 + \tau$, then F will equal 1 for all time such that $t \geq 1 + \tau$, and the steady-state TAL concentration profile will persist, provided that the system remains unperturbed.

Under the assumption of no solute backleak, the steady-state TAL concentration profile of C, denoted by $S(x)$, is given by the solution of the ODE

$$S'(x) = -J(S(x)), \quad S(0) = 1, \tag{2.4}$$

where we have used $F(S(1)) = F(C_{op}) = 1$ and $S(0) = C(0,t) = 1$, and where the prime indicates differentiation with respect to x.

Normalization of equations. The dimensional forms of Eqs. 2.1 and 2.2 are given by

$$\begin{aligned} \frac{\partial}{\partial t}C(x,t) = &-\frac{F(C(1,t-\tau))}{\pi r^2}\frac{\partial}{\partial x}C(x,t) \\ &-(2/r)\left(\frac{V_{max}C(x,t)}{K_M + C(x,t)} + P\left(C(x,t) - C_e(x)\right)\right), \end{aligned} \tag{2.5}$$

and

$$F(C(L,t-\tau)) = \alpha\left(Q_{op} + \frac{\Delta Q}{2}\tanh\left(\frac{k}{2}\left(C_{op} - C(L,t-\tau)\right)\right)\right), \tag{2.6}$$

where r is the tubular radius, α is the (dimensionless) fraction of single nephron glomerular filtration rate (SNGFR) reaching the TAL, Q_{op} is the steady-state (operating) SNGFR, ΔQ is the TGF-mediated range of SNGFR, and k is the sensitivity of the TGF response [13]. To express these equations in nondimensional form, let $\tilde{x} = x/L$, $\tilde{t} = t/t_o$, $\tilde{\tau} = \tau/t_o$, $\tilde{r} = r/\sqrt{A_o/\pi}$, $\tilde{C}(\tilde{x},\tilde{t}) = C(x,t)/C_o$, $\tilde{C}_e(\tilde{x}) = C_e(x)/C_o$, $\tilde{F}(\tilde{C}(1,\tilde{t}-\tilde{\tau})) = F(C(L,t-\tau))/F_o$, $\tilde{V}_{max} = V_{max}/(V_{max})_o$, $\tilde{K}_M = K_M/C_o$, $\tilde{P} = P/P_o$, $K_1 = \Delta Q/2Q_o$, $K_2 = kC_o/2$, and $\tilde{C}_{op} = C_{op}/C_o$, where L is TAL length, and where the quantities subscripted with an "o" are conveniently chosen reference values: $A_o = \pi r^2$, $t_o = A_oL/F_o$, $C_o = C(0,t)$ (assumed constant), $F_o = F_{op} = \alpha Q_{op}$, $(V_{max})_o = F_oC_o/(2\pi rL)$, $P_o = F_o/(2\pi rL)$, and $Q_o = Q_{op}$. With these conventions, t_o is the filling time (and thus the transit time) of the TAL at flow rate F_o, and $(V_{max})_o$ is the rate of solute advection into the inlet of the TAL at flow rate F_o, divided by the area of the sides of the TAL. When Eqs. 2.5 and 2.6 are rewritten in dimensionless terms and the tilde symbols are dropped, Eqs. 2.1 and 2.2 follow directly.

Model parameters. The values of model base-case parameters, assuming no chloride backleak, are given in Table 1; the criteria for their selection and supporting references were given in Ref. [13]. The steady-state operating concentration C_{op} was calculated numerically using the TAL dimensions and transport parameters, with steady flow $F = 1$ in Eq. 2.1.

Table 1: *Parameter set for no chloride backleak ($P = 0$)*

Parameter	Value
α	0.200 (dimensionless)
C_o	275 mM
L	0.500 cm
Q_{op}	30.0 nl/min
ΔQ	18.0 nl/min
r	10.0 μm
t_o	15.708 s
τ	3.5 s
K_M	140 mM
V_{max}	17.3 nmole $\cdot$ cm^{-2} $\cdot$ s^{-1}
C_{op}	32.12 mM

2.2. Bifurcation analysis. Under normal conditions, renal blood flow is subject to disturbances from a number of physiological sources, such as heartbeat, respiration, stress, activity, and other factors that cause fluctuations in blood pressure. Such disturbances will result in deviations from time-independent steady-state intratubular nephron flow. Thus, an important question is, What is the behavior of a nephron subsequent to a transient perturbation of that steady state? In the context of the minimal nephron model, an answer to this question was provided in Ref. [13]: if the system is perturbed, the stable solution depends on the time delay τ and on the gain of the feedback loop (the gain will be determined below).[2] In one region of the delay–gain parameter plane, the perturbed solution tends back to the steady-state. In another region, the steady state is no longer stable and the perturbed solution tends to a regular oscillation, i.e., to an LCO. The two regions in the delay–gain parameter space are separated by a curve, and that curve is the locus of a bifurcation where the time-independent steady-state solution loses stability and the steady state is replaced by a stable LCO (see Fig. 2, below).

In this subsection, we summarize the analysis that predicts the bifurcation from a stable time-independent steady-state to a stable LCO. We first combine Eqs. 2.1 and 2.2 into a single equation, which we linearize by assuming a solution of the form

$$C(x,t) = S(x) + \epsilon D(x,t), \tag{2.7}$$

where, recall, $S(x)$, the solution of Eq. 2.4, is the steady-state TAL concentration profile, and where D represents the deviation from that steady state. To obtain the linearization, expand (by means of a Taylor series in

[2] A physiological perturbation can be simulated by a transient augmentation of flow, an augmentation which may be achieved by adding a small quantity to the right-hand side of Eq. 2.2.

ϵ) those terms that are nonlinear in ϵ, retaining only the terms that are first order in ϵ. This yields a PDE for the deviation, given by

$$\frac{\partial}{\partial t}D(x,t) = -\frac{\partial}{\partial x}D(x,t) \\ -J'(S(x))D(x,t) - F'(C_{op})S'(x)D(1,t-\tau), \tag{2.8}$$

where the primes indicate differentiation with respect to the arguments of the functions. (The terms that are order zero in ϵ drop out because they are equivalent to the time-independent steady-state ODE for $S(x)$, i.e., to Eq. 2.4.) Because $C(0,t) = S(0) = 1$, the boundary condition for $D(x,t)$ is

$$D(0,t) = 0. \tag{2.9}$$

If the deviation arising from a perturbation of the steady-state diminishes in time, i.e., if the deviation tends to zero in the sense that

$$\lim_{t\to\infty}\left(\max_{x\in[0,1]}|D(x,t)|\right) = 0, \tag{2.10}$$

then the time-independent steady-state solution $S(x)$ is the stable solution. On the other hand, if D does not tend to zero, then S is an unstable solution and the stable solution has a TAL concentration profile that varies in time.

We assume that the deviation D can be written as a product of a function $f(x)$ that depends only on the spatial variable x and an exponential function $e^{\lambda t}$ that depends only on the temporal variable t. Thus we use the method of separation of variables, and we write

$$D(x,t) = f(x)e^{\lambda t}, \tag{2.11}$$

where $f(0) = 0$ to conform to the boundary condition given by Eq. 2.9. Because the parameter λ can have both a real part (Re λ) and an imaginary part (Im λ), $e^{\lambda t}$ can both modify the amplitude of D and allow oscillations in D.

If Re $\lambda < 0$, then D tends to zero in the sense of Eq. 2.10, and the steady-state solution $S(x)$ is the stable TAL concentration profile. However, if Re $\lambda > 0$, then a perturbation of the steady state may lead to an oscillatory solution of Eq. 2.8, and, indeed, to oscillations that grow without bound. However, in the full model, nonlinearities in Eqs. 2.1 and 2.2 (specifically, nonlinearities in the bounded range of F and in the Michaelis Menten kinetics) prevent unbounded oscillations.

If one assumes that the form for D given in Eq. 2.11 is a solution of the linear PDE given by Eq. 2.8, then that PDE imposes a relationship between λ and the parameters arising in the PDE. That relationship is the characteristic equation, which we now derive. If one substitutes the

assumed form for D into into Eq. 2.8 and cancels the common factor of $e^{\lambda t}$, the result is a first-order linear ODE for $f(x)$ given by

$$f'(x) = -\Big(\lambda + J'(S(x))\Big) f(x) + K_1 K_2 S'(x) f(1) e^{-\lambda\tau}, \tag{2.12}$$

where the primes indicate differentiation with respect to the arguments of the functions, and where $F'(C_{op})$ has been replaced by $-K_1K_2$. The solution to this ODE can be written as

$$f(x) = K_1 K_2 f(1) e^{-\lambda\tau} e^{-h(x)} \int_0^x S'(y) e^{h(y)}\, dy \tag{2.13}$$

where

$$h(x) = \int_0^x \Big(\lambda + J'(S(u))\Big)\, du. \tag{2.14}$$

By differentiating equation Eq. 2.4 with respect to x, one obtains $J'(S(x)) = -S''(x)/S'(x)$, and therefore $h(x) = \lambda x - \ln|S'(x)|$. Thus, after simplification, Eq. 2.13 can be written as

$$f(x) = -K_1 K_2 f(1) e^{-\lambda\tau} S'(x) \left(\frac{e^{-\lambda x} - 1}{\lambda}\right). \tag{2.15}$$

If one evaluates this equation at $x = 1$, cancels $f(1)$ from both sides, and defines a new, positive parameter γ by

$$\gamma = -K_1 K_2 S'(1), \tag{2.16}$$

then one obtains the characteristic equation for λ,

$$1 = \gamma e^{-\lambda\tau} \left(\frac{e^{-\lambda} - 1}{\lambda}\right). \tag{2.17}$$

This equation contains two dimensionless parameters: τ, the normalized time delay, and γ, the feedback loop gain. The gain is a measure of the signal amplification by the feedback loop. (An in-depth treatment of gain is given in Ref. [14]; technically speaking, $-\gamma$ is the gain whereas γ is the gain magnitude, because gain in a negative feedback system is negative.)

The complex-valued parameter λ can be written $\lambda = \zeta + i\omega$, where ζ and ω are real numbers with Re $\lambda = \zeta$ and Im $\lambda = \omega$. The sign of ζ determines whether the amplitude of the oscillatory solution is decreasing or increasing. To determine a bifurcation locus separating increasing solution amplitudes from decreasing ones, set $\zeta = 0$ (i.e., let $\lambda = i\omega$). After algebraic transformations, the characteristic equation can then be written as

$$\omega/2 = -\gamma \sin(\omega/2) \Big(\cos(\omega(\tau + 1/2)) - i \sin(\omega(\tau + 1/2))\Big). \tag{2.18}$$

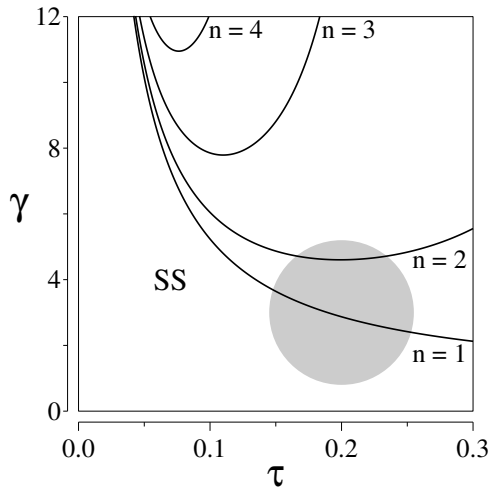

FIG. 2. *Bifurcation curves γ_n given by Eq. 2.21, for n = 1, 2, 3, and 4. In the region indicated by* "SS" *a solution obtained by a transient perturbation of the time-independent steady-state solution will converge back to the steady-state solution. However, above the curve labeled by* "n = 1" *a transient perturbation of the time-independent steady-state will result in a solution that oscillates in time. The gray disk indicates the approximate region that corresponds to parameters for normotensive rats.*

The imaginary part of Eq. 2.18,

$$0 = \gamma \sin(\omega/2) \sin(\omega(\tau + 1/2)), \tag{2.19}$$

implies that either $\frac{\omega}{2} = n\pi$ or $\omega(\tau + \frac{1}{2}) = n\pi$, where n is an integer. The first alternative, when substituted into Eq. 2.18, implies that $\omega = 0$ and $n = 0$, which corresponds to the steady-state solution. The second alternative,

$$\omega = \frac{n\pi}{\tau + 1/2}, \quad n = 1,\ 2,\ 3, \ldots \tag{2.20}$$

corresponds to time-dependent oscillatory solutions. Substituting Eq. 2.20 into the real part of the Eq. 2.18 yields

$$\gamma_n = (-1)^{n+1} \frac{n\pi/(2\tau + 1)}{\sin(n\pi/(2\tau + 1))}, \quad n = 1,\ 2,\ 3, \ldots \tag{2.21}$$

This equation defines the bifurcation curves on the τ-γ plane; portions of some of those curves are shown in Fig. 2.

For each parameter pair (τ, γ) on any of these curves, the linearized model equation (Eq. 2.8) has a periodic, standing-wave solution with the frequency given by Eq. 2.20. For a fixed τ, the frequency of the periodic solution corresponding to the n^{th} bifurcation curve is n times the lowest possible frequency.

We now restrict attention to the curve labeled $n = 1$, which we call the primary bifurcation curve (or primary bifurcation locus). In Ref. [13], analysis demonstrated that $\partial\zeta/\partial\gamma > 0$ on this curve, and, by construction, $\zeta = 0$ on this curve. Thus, as the parameter pair (τ, γ) crosses the curve from the lower to the upper region, the sign of ζ changes from negative to positive. Below and to the left of the $n = 1$ curve, all solutions of Eq. 2.8 of the form Eq. 2.11 have Re $\lambda < 0$, and the perturbation $D(x, t)$ diminishes to zero over time, in the sense of Eq. 2.10. However, above the primary bifurcation curve, the deviation D arising from a perturbation will tend to increase in amplitude. The change in solution behavior across the curve $n = 1$ suggests that a Hopf bifurcation occurs at this locus (see additional detail on this point in Ref. [13]).

When one applies the results of this linear analysis to the nonlinear system given by Eqs. 2.1 and 2.2, one expects that in the region under the primary bifurcation curve ($n = 1$), the time-independent steady-state will be the only stable solution; but in the region above that curve, an LCO will be the only stable solution. Numerical simulations have confirmed this expectation; for details, see Ref. [13].

3. The Reduced Model. In this section we derive the reduced model from the minimal model summarized above in subsection 2.1. The reduced model eliminates the PDE that appears in the minimal model and thus the space dependence inherent in that PDE, but it retains the time dependence and the effects of the delay. This reduced model, which is a linearization of the characteristic form of the hyperbolic PDE given by Eq. 2.1, provides an explicit formula for the TAL flow rate in terms of the history of that flow rate. Although the reduced model depends on the elimination of solute backleak and on two linearizations, the reduced model may nonetheless provide an adequate approximation to the minimal model in some contexts.

3.1. Model derivation. Along the characteristic curves determined by

$$\frac{d}{dt}x(t) = F(C(1, t - \tau)), \tag{3.1}$$

the equation for chloride conservation (Eq. 2.1) takes the form

$$\frac{d}{dt}C(x(t), t) = -J(C(x(t), t)), \tag{3.2}$$

provided that solute backleak is taken to be zero i.e., provided that $P = 0$. (The relationship of Eqs. 3.1 and 3.2 to Eq. 2.1 can be seen by computing the total derivative on the left side of Eq. 3.2 and comparing the result with Eq. 2.1, while recalling J in Eq. 2.3. The requirement that $P = 0$ is explained below in Section 3.2.)

In Eqs. 3.1 and 3.2, which are said to be in characteristic form, the dependent variables can be parameterized by the time variable. To see this,

and to simplify notation, define functions $\mathcal{F}$ and $\mathcal{C}$ by

$$\mathcal{F}(t) \equiv F(C(1, t-\tau)) \tag{3.3}$$

and

$$\mathcal{C}(t) \equiv C(x(t), t). \tag{3.4}$$

Also, define $T_x(t)$ be the TAL transit transit time from $x = 0$ to position $x \in [0, 1]$ at time t. This transit time is the time required for a particle that is moving with the flow to traverse the portion of the model TAL that extends from 0 to x.

By integrating Eq. 3.1, one obtains an implicit equation for T_x,

$$x(t) = \int_{t-T_x(t)}^{t} \mathcal{F}(s)\ ds, \tag{3.5}$$

where $t - T_x(t)$ is the time at which a particle of fluid currently located at $x(t)$ entered the TAL. By evaluating Eq. 3.5 at $x = 1$ and defining the transit time up the TAL from $x = 0$ to the MD by $T_{MD}(t) \equiv T_x(t)$ with $x = 1$, one obtains

$$1 = \int_{t-T_{MD}(t)}^{t} \mathcal{F}(s)\ ds. \tag{3.6}$$

By replacing $C(x(t), t)$ in Eq. 3.2 with $\mathcal{C}(t)$ and solving Eq. 3.2 along the characteristic curves in the $x - t$ plane specified by Eq. 3.1, subject to the boundary condition at the TAL entrance, $\mathcal{C}(0) = C(0, t) = 1$, one obtains the concentration $\mathcal{C}(T_x(t))$. By comparing Eq. 3.2 with Eq. 2.4, one sees that $\mathcal{C}(T_x)$ is exactly $S(T_x)$, where S is the solution of the steady-state ODE given in Eq. 2.4.

To obtain a tractable equation for the flow rate, linearize $\mathcal{C}$ (by means of the first two terms of a Taylor series) about the steady-state TAL transit time $T_{MD} = 1$ to find

$$\mathcal{C}(T_{MD}(t)) \approx \mathcal{C}(1) + (T_{MD}(t) - 1)\mathcal{C}'(1). \tag{3.7}$$

Note that $\mathcal{C}(1) = S(1) = C_{op}$ and $\mathcal{C}'(1) = S'(1)$. By using the linearization Eq. 3.7 and the gain as expressed in Eq. 2.16, one can substitute into Eqs. 2.2 and 3.3 to obtain

$$\mathcal{F}(t) \approx 1 + K_1 \tanh\left(\frac{\gamma}{K_1}\left(T_{MD}(t-\tau) - 1\right)\right). \tag{3.8}$$

An additional linearization is required to complete the derivation. Consider Eq. 3.5 as an implicit equation for transit time T_x, i.e., let $x = g(T_x)$, where

$$g(T_x) = \int_{t-T_x(t)}^{t} \mathcal{F}(s)\ ds. \tag{3.9}$$

Now set $x = 1$ so that $T_x = T_{MD}$, and linearize $g(T_{MD})$ (with respect to its argument T_{MD}), by expanding in a Taylor series to first order about $T_{MD} = 1$ (with t considered fixed), to obtain

$$1 = g(T_{MD}) \approx g(1) + (T_{MD}(t) - 1)g'(1) \approx \int_{t-1}^{t} \mathcal{F}(s)\ ds + (T_{MD}(t) - 1)\mathcal{F}(t-1). \tag{3.10}$$

By solving this equation for T_{MD}, one obtains

$$T_{MD}(t) \approx 1 + \frac{1 - \int_{t-1}^{t} \mathcal{F}(s)\ ds}{\mathcal{F}(t-1)} = 1 + \frac{\int_{t-1}^{t} (1 - \mathcal{F}(s))\ ds}{\mathcal{F}(t-1)}\ . \tag{3.11}$$

To obtain the reduced model, consider the linearizations in Eqs. 3.8 and 3.11 to be exact. By substituting Eq. 3.11 for $T_{MD}(t)$ in Eq. 3.8, one obtains

$$\mathcal{F}(t) = 1 + K_1 \tanh\left(\frac{\gamma \int_{t-\tau-1}^{t-\tau} (1 - \mathcal{F}(s))\ ds}{K_1 \mathcal{F}(t-\tau-1)}\right). \tag{3.12}$$

This equation, which constitutes the reduced TGF model, expresses the TAL flow rate $\mathcal{F}$ at time t as a function of average flow over a fixed interval of past time. Fixing this interval of integration greatly simplifies numerical computations.

3.2. Bifurcation analysis and numerical results. The reduced TGF model given by Eq. 3.12 expresses the TAL fluid flow rate in terms of the flow rate history. This model formulation avoids explicit consideration of the spatially varying TAL chloride concentration $C(x,t)$. Instead, the information provided in the minimal model by the concentration at the MD (i.e., $C(1,t)$) is approximated in the reduced model by information about the flow rate $\mathcal{F}$ in the interval $[t-\tau-1, t-\tau]$, viz., the average of that flow divided by the value of that flow at time $t-\tau-1$.

We now ask, As an approximation of the minimal model, how accurate is the reduced model? More specifically, is the principal bifurcation locus changed? Although the reduced model avoids an explicit model representation of the TAL, it contains the same two bifurcation parameters, τ and γ, as the minimal model. In the reduced model, these parameters retain the same meaning as in the minimal model, and their normalizations are unchanged. Because the characteristic equation for the minimal model is based on a linearization procedure, and because the derivation of the reduced model is based on two linearizations, one might reasonably expect that a bifurcation analysis of the reduced model would result in the same bifurcation loci as found in the minimal model. We confirm this expectation by assuming a solution $\mathcal{F}(t)$ of Eq. 3.12 in the form of a small deviation from steady-state flow 1, i.e., we set

$$\mathcal{F}(t) = 1 + \epsilon D(t), \tag{3.13}$$

where ϵ is a small parameter. By substituting this form of $\mathcal{F}(t)$ into Eq. 3.12 and linearizing in ϵ, one obtains

$$D(t) = -\gamma \int_{t-\tau-1}^{t-\tau} D(s)\ ds. \tag{3.14}$$

If, in analogy with Eq. 2.11, we let $D(t)$ take the form of a complex exponential $D(t) = e^{\lambda t}$ and evaluate the resulting integral in Eq. 3.14, the characteristic equation is found to be

$$1 = -\gamma e^{-\lambda\tau} \left(\frac{1 - e^{-\lambda}}{\lambda} \right). \tag{3.15}$$

This characteristic equation is identical to the characteristic equation derived in Section 2.2 for the minimal model, i.e., Eq. 3.15 is the same equation as Eq. 2.17.

For flow rates sufficiently close to the steady-state flow rate, and for parameter values sufficiently close to the usual operating point (corresponding to the parameters of Table 1), numerical studies confirm that the behavior of the reduced model is very similar to that of the minimal model. Figure 3 contains representative results for values of gain γ ranging from 2 to 6, and for a dimensional time delay τ of about 3.5 s. For this delay, the dimensionless value of τ (found by dividing by the steady-state TAL transit time 15.708 s), to three significant digits, is 0.223, which was the value used in the calculations. Equation 2.21 gives a corresponding critical gain value of $\gamma_c = 2.6357$. In each panel of Fig. 3, the same numerical experiment was conducted for both the reduced and the minimal model. In each experiment, the time-independent steady-state was perturbed at $t = 0$ by a transient step in fluid flow, of amplitude 0.06 nl/min (1% of steady-state TAL flow) and of duration 15.708 seconds (the steady-state TAL transit time t_o).

Panels A and B of Fig. 3, for γ equals 2 and 3, respectively, show close agreement between the two models and, in addition, exhibit representative model behavior for gains that bound the critical gain ($\gamma_c = 2.6357$). Additional numerical calculations (not shown) indicate that when $\gamma = 2.6300$, which is slightly less than γ_c, the qualitative behavior of both models closely resembles the behavior shown in panel A, except that the amplitude of the oscillations decreases much more slowly for $\gamma = 2.6300$ than for $\gamma = 2$. For $\gamma = 2.6400$, which slightly exceeds γ_c, the qualitative behavior of both models closely resembles the behavior shown in panel B, except that the amplitude increases much more slowly for $\gamma = 2.6400$ than for $\gamma = 3$.

Panels C and D, for the larger gains of 4 and 6, respectively, show good qualitative agreement between the two models. For these gain values, the phase shift between the two models' results is established in the early seconds and then persists. The shapes of the waveforms are similar, and the amplitudes are also similar. In panel C ($\gamma = 4$), the amplitude for

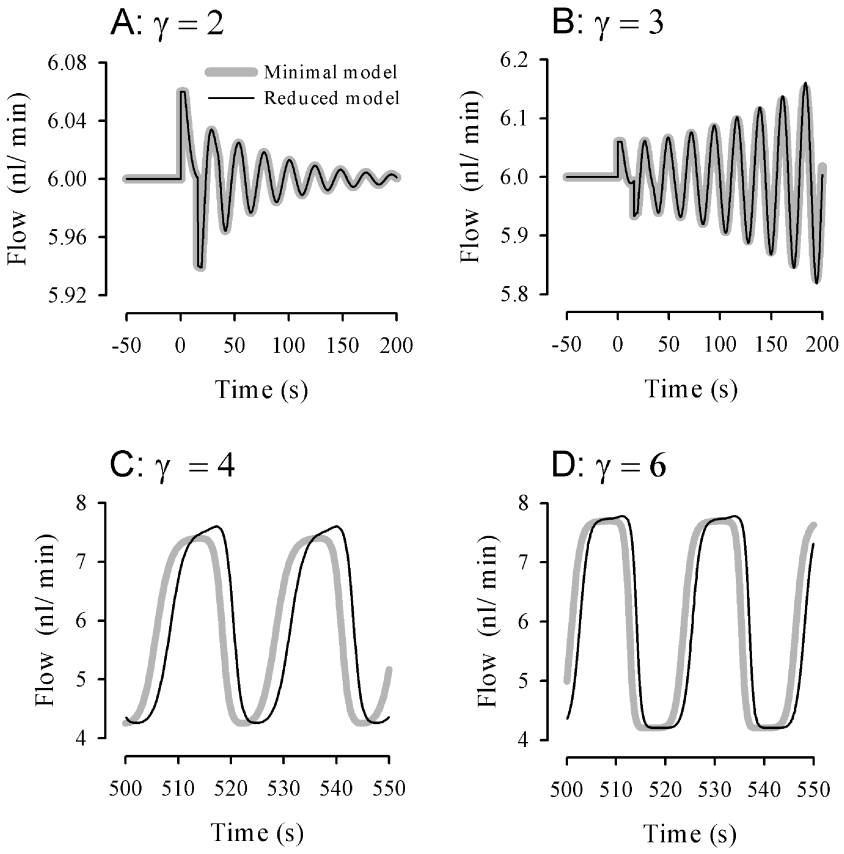

FIG. 3. *Numerical results of flow $\mathcal{F}$ as a function of time t for both the reduced model and the minimal model. The results, for gain values γ = 2, 3, 4, and 6, were computed with the parameters in Table 1. Results from the reduced model are indicated by the thin black line; results from the minimal model are indicated by the thick gray line. This figure provides numerical evidence that the reduced model provides a good approximation to the minimal model.*

the reduced model exceeds that for the minimal model by less than 6.2%; in panel D ($\gamma = 6$), the amplitudes are more nearly the same, since the extrema of the oscillations in both cases are approaching the extrema imposed by the choice of ΔQ given in Table 1 (i.e., approaching 4.2 and 7.8 nl/min).

The error incurred by using the reduced model, when considered as an approximation for the minimal model, arises in part from the fixed interval of integration in Eq. 3.12, which is a consequence of the linearization given by Eq. 3.10. That equation calculates the average flow over a (dimensionless) unit of time corresponding to one steady-state TAL transit time,

whereas the flow should be averaged over the actual transit time of fluid to the MD, as specified implicitly in Eq. 3.6. Thus, the fixing of the interval of integration in the reduced model provides a substantial simplification, but it diminishes the fidelity of the model to the physics of the physiological process that is being represented.

The other source of error in the reduced model, as compared to the minimal model, arises from the linearization in Eq. 3.7: using only the steady-state concentration at the MD (i.e., $S(1)$) and the derivative of that concentration at the MD (i.e., $S'(1)$), the concentration at the MD is expressed in Eq. 3.7 as a linear function of transit time. Thus the reduced model does not depend on the details of the transport kinetics, but only on local steady-state information at the MD.

In obtaining the reduced model, we have assumed that the TAL transepithelial transport is homogeneous in space, and this assumption is required in the derivation of the reduced model. If one instead assumes that there is a solute backleak, formulated to depend on a spatially-varying external concentration (as in Eq. 2.1), then the TAL concentration at the MD is no longer a function of transit time only but also of the trajectory in space: the MD concentration depends on how long the fluid at the MD is near particular sites along the TAL, i.e., on where the fluid "spends its time" along the TAL.[3]

Numerical solutions to the reduced model are easily computed. Given a history of the flow $\mathcal{F}$ in the interval $[t-\tau-1, t)$, the flow for $t \in [t, t+\tau)$ can be approximated by repeated application of the trapezoidal rule to solve the integral in Eq. 3.12. It is unnecessary to numerically recompute the sum that represents the integral at each new time step Δt. Instead, one can add to that sum the information for the new step at time t (i.e., the term containing the approximation for $\mathcal{F}(t-\tau+\Delta t)$), and subtract the most time-retarded step (i.e., the term containing the approximation for $\mathcal{F}(t-\tau-1)$).

This method of solution, which can be applied even as τ tends to zero, involves a bootstrapping of information, inasmuch as the information that is computed for each new interval of duration τ is then used (along

[3]If the backleak permeability P does not equal zero, then the equations analogous to Eq 3.2 and Eq. 2.4, have the forms $\frac{d}{dt}C(x(t),t) = -J(C(x(t),t), C_e(x(t)))$ and $\frac{d}{dx}S(x) = -J(S(x), C_e(x))$, respectively, where the backleak term has been notationally incorporated into J. From these equations one sees that transepithelial transport is no longer homogeneous in space through dependence on C (or S), but, instead, has a spatial dependence through $C_e(x)$. Therefore, the TAL luminal concentration $C(x,t)$ depends not only on the transit time (the integral of the particle trajectory $\mathcal{F}(t)$), but also on the particle trajectory $\mathcal{F}(t)$ along the TAL as a function of time; thus, in general, C is not a function of the transit time T_x only, and one cannot, in general, write an expression of the form $\mathcal{C}(T_x(t)) = C(x,t)$. Moreover, if $P \neq 0$, then $S(T_x)$ will be a correct expression for concentration only in special cases, e.g, constant flow speed $\mathcal{F} = 1$. Thus, one cannot generally assert the equality $\mathcal{C}(T_x) = S(T_x)$, an equality that is essential to obtaining Eq. 3.8.

with already existing information in the previous nondimensional interval of duration 1) to compute the solution in the next interval of duration τ. The numerical solutions exhibited in Fig. 3 were obtained by means of this method.

It is especially noteworthy that numerical solutions to the reduced model can be obtained much more rapidly than can comparable solutions to the minimal model. Obtaining solutions to the minimal model by solving the delay PDE directly (i.e., Eq. 2.1, with $P = 0$), involves computing a new TAL profile on the interval $[0, 1]$ at each new time step. High spatial and temporal resolution is required in such calculations to obtain acceptable accuracy [16]. An alternative method for the minimal model, using Eqs. 2.2, 3.2, and 3.6, is more efficient, but nonetheless involves solving numerically the implicit condition for T_{MD} given by Eq. 3.6, and, if Michaelis-Menten kinetics is employed, solving an implicit equation arising from Eq. 3.2 (viz., Eq. 7, for $x = 1$, in Ref. [15]).

4. Functional ordinary differential equation formulation. In this section we derive a formulation of the minimal model that eliminates the space dependence and represents model behavior as a functional ODE for T_{MD}, the TAL transit time to the MD. The functional ODE formulation can be regarded as a conceptual bridge between the minimal model and reduced model, and thus this formulation can assist in understanding why the reduced model allows for significant computational simplification.

To obtain the functional ODE formulation, differentiate Eq. 3.6 to obtain

$$0 = \mathcal{F}(t) - \mathcal{F}(t - T_{MD}(t)) \left(1 - \frac{d}{dt} T_{MD}(t)\right). \tag{4.1}$$

Then solve for dT_{MD}/dt to obtain

$$\frac{d}{dt} T_{MD}(t) = 1 - \frac{\mathcal{F}(t)}{\mathcal{F}(t - T_{MD}(t))}, \tag{4.2}$$

and recall the definitions for $\mathcal{F}$ and $\mathcal{C}$ (Eqs. 3.3 and 3.4), and the material following Eq. 3.6, to obtain the dependence of F on T_{MD},

$$\mathcal{F}(t) = F(C(1, t - \tau)) = F(\mathcal{C}(T_{MD}(t - \tau))). \tag{4.3}$$

To write the ODE in terms of $T_{MD}(t)$, substitute equation Eq. 4.3 into Eq. 4.2, and let $S = \mathcal{C}$ to obtain

$$\frac{d}{dt} T_{MD}(t) = 1 - \frac{F(S(T_{MD}(t - \tau)))}{F(S(T_{MD}(t - \tau - T_{MD}(t))))}. \tag{4.4}$$

Because the nondimensional steady-state value for T_{MD} is 1, and the functional ODE is space-independent, we may let $T_{MD}(t) = 1 + \epsilon D(t)$, where D, the deviation analogous to that first used in Eq. 2.7, is given

by $D(t) = e^{\lambda t}$. If one linearizes in ϵ, one obtains the same characteristic equation as obtained twice previously, viz., Eqs. 2.17 and 3.15. Therefore, the stable solution of this problem is determined by exactly the same conditions for τ and γ that were previously determined in Sections 2.2 and 3.2. This is the expected result since the functional ODE represents the same behavior as the minimal model. Indeed, from the solution to the ODE, the flow F and concentration $C(1,t)$ at time t can be recovered as $F(S(T_{MD}(t-\tau)))$ and $S(T_{MD}(t))$, respectively.

The initial condition that provides a time-independent steady-state for this ODE, a condition that is analogous to the steady-state initial conditions for the minimal problem, is the condition that $T_{MD} \equiv 1$ for $t \in [-\tau - 1, 0]$. If the ODE remains unperturbed, the steady-state solution will persist for $t > 0$.

The significance of the functional ODE formulation given by Eq. 4.4, in the context of the reduced model, is that it provides additional insight into the advantages of using the reduced model for computation. Although the functional ODE is space independent like the reduced model, it is an alternative formulation of the minimal model, a formulation that shows that the rate of change of the transit time depends on the transit time at the previous time $t - \tau$ and also at the previous time $t - \tau - T_{MD}(t)$, which, of course, depends on the current transit time $T_{MD}(t)$. An accurate numerical solution of the functional ODE formulation would require a very precise estimation of two previous transit times at each time step; these delay times must be determined by interpolation since they will generally fall at times that do not coincide with the time increments of the numerical calculation. A comparison of this ODE formulation with the reduced model gives emphasis to the conceptual and computational simplicity of the reduced model, relative to the minimal model. The ODE formulation of the minimal model may be helpful, however, for theoretical investigation of the minimal model.

5. Summary and Conclusion. We have derived a model—the reduced model—that approximates the "minimal" model that we previously developed for the tubuloglomerular feedback loop [13]. The reduced model has the same characteristic equation as the minimal model, which means that, with regard to its stable behavior (time-independent steady-state versus limit-cycle oscillations), the reduced model has the same principal bifurcation boundary in parameter space as does the minimal model. Moreover, numerical simulations show that the reduced model has quantitative behavior that closely approximates that of the minimal model, a finding that is of especial significance because the computational time required to compute numerical results for the reduced model is much less than that required for analogous results from the minimal model.

An important potential application of the reduced model is the study of the effects of nephron-nephron coupling on renal dynamics in large pop-

ulations of nephrons. Indeed, the simplicity of the reduced model offers the possibility of more easily applying analytical methods to the study of large systems of coupled nephrons [19]. Such coupling, found in physiological experiments [7, 12], may contribute to the complex flow dynamics observed by Yip and colleagues [5, 22]. A more complete understanding of single nephron and coupled nephron dynamics, by means of the minimal model, the reduced model presented here, or other pertinent model formulations, is a principal objective of our work.

Acknowledgments

We thank Anita T. Layton for technical assistance and for a careful reading of this manuscript.

This research was supported in part by the National Institutes of Health (National Institute of Diabetes and Digestive and Kidney Diseases, grant DK-42091).

REFERENCES

[1] Barfred, M., E. Mosekilde, and N.-H. Holstein-Rathlou. Bifurcation analysis of nephron pressure and flow regulation. *Chaos* 6: 280-287, 1996.

[2] Bellman, R. E., and K. L. Cooke. *Differential-Difference Equations.* New York: Academic Press, 1963.

[3] Casellas, D., M. Dupont, N. Bouriquet, L. C. Moore, A. Artuso, and A. Mimran. Anatomic pairing of afferent arterioles and renin cell distribution in rat kidneys. *Am. J. Physiol.* 267 (*Renal Fluid Electrolyte Physiol.* 36): F931-F936, 1994.

[4] Casellas, C., and L. C. Moore. Autoregulation and tubuloglomerular feedback in juxtamedullary glomerular arterioles. *Am. J. Physiol.* 258 (*Renal Fluid Electrolyte Physiol.* 27): F660–F669, 1990.

[5] Chen, Y.-M, K.-P. Yip, D. J. Marsh, and N.-H. Holstein-Rathlou. Magnitude of TGF-initiated nephron-nephron interactions is increased in SHR. *Am. J. Physiol.* 269 (*Renal Fluid Electrolyte Physiol.* 38): F198-F204, 1995.

[6] Hale, J. K., and S. M. Verduyn Lunel. *Introduction to Functional Differential Equations.* New York: Springer-Verlag, 1993.

[7] Holstein-Rathlou, N.-H. Synchronization of proximal intratubular pressure oscillations: evidence for interaction between nephrons. *Pflügers Arch.* 408: 438-443, 1987.

[8] Holstein-Rathlou, N.-H., and P. P. Leyssac. Oscillations in the proximal intratubular pressure: a mathematical model. *Am. J. Physiol.* 251 (*Renal Fluid Electrolyte Physiol.* 21): F560–F572, 1987.

[9] Holstein-Rathlou, N.-H., and D. J. Marsh. Oscillations of tubular pressure, flow, and distal chloride concentration in rats. *Am. J. Physiol.* 256 (*Renal Fluid Electrolyte Physiol.* 25): F1007-F1014, 1989.

[10] Holstein-Rathlou, N.-H., and D. J. Marsh. A dynamic model of the tubuloglomerular feedback mechanism. *Am. J. Physiol.* 258 (*Renal Fluid Electrolyte Physiol.* 27): F1448–F1459, 1990.

[11] Holstein-Rathlou, N.-H., and D. J. Marsh. Renal blood flow regulation and

arterial pressure fluctuations: a case study in nonlinear dynamics. *Physiol. Rev.* 74: 637–681, 1994.

[12] Just, A., U. Wittman, H. Ehmke, and H. R. Kirchheim. Autoregulation of renal blood flow in the conscious dog and the contribution of the tubuloglomerular feedback. *J. Physiol.* 506.1: 275-290, 1998.

[13] Layton, H. E., E. B. Pitman, and L. C. Moore. Bifurcation analysis of TGF-mediated oscillations in SNGFR. *Am. J. Physiol.* 261 (*Renal Fluid Electrolyte Physiol.* 30): F904-F919, 1991.

[14] Layton, H. E., E. B. Pitman, and L. C. Moore. Instantaneous and steady-state gains in the tubuloglomerular feedback system. *Am. J. Physiol.* 268 (*Renal Fluid Electrolyte Physiol.* 37): F163-F174, 1995.

[15] Layton, H. E., E. B. Pitman, and L. C. Moore. Nonlinear filter properties of the thick ascending limb. *Am. J. Physiol.* 273 (*Renal Fluid Electrolyte Physiol.* 42): F625–F634, 1997.

[16] Layton, H. E., E. B. Pitman, and L. C. Moore. Spectral properties of the tubuloglomerular feedback system. *Am. J. Physiol.* 273 (*Renal Fluid Electrolyte Physiol.* 42): F635–F649, 1997.

[17] Layton, H. E., E. B. Pitman, and L. C. Moore. Limit-cycle oscillations and tubuloglomerular feedback regulation of distal sodium delivery. *Am. J. Physiol. Renal Physiol.* 278: F287-F301, 2000.

[18] Pitman, E. B., and H. E. Layton. Tubuloglomerular feedback in a dynamic nephron. *Commun. Pure Appl. Math.* 42: 759–787, 1989.

[19] Pitman, E. B., R. M. Zaritski, L. C. Moore, and H. E. Layton. Tubuloglomerular feedback-mediated oscillations in two coupled nephrons. Preprint.

[20] Schnermann, J., and J. P. Briggs. Function of the juxtaglomerular apparatus: control of glomerular hemodynamics and renin secretion. In: *The Kidney: Physiology and Pathophysiology* (3d ed.), edited by D. W. Seldin and G. Giebisch. Philadelphia: Lippincott Williams & Wilkins, 2000, p. 945–980.

[21] Vander, A. J. *Renal Physiology*, 5th ed. New York: McGraw-Hill, 1995.

[22] Yip, K.-P., N.-H. Holstein-Rathlou, and D. J. Marsh. Chaos in blood flow control in genetic and renovascular hypertensive rats. *Am. J. Physiol.* 261 (*Renal Fluid Electrolyte Physiol.* 30): F400-F408, 1991.

[23] Yip, K.-P., N.-H. Holstein-Rathlou, and D. J. Marsh. Dynamics of TGF-initiated nephron-nephron interactions in normotensive rats and SHR. *Am. J. Physiol.* 262 (*Renal Fluid Electrolyte Physiol.* 31): F980-F988, 1992.

[24] Zaritski, R. M. Models of complex dynamics in glomerular filtration rate. Ph.D. diss., State University of New York, Buffalo, New York, 1999.